

Review

High-Harmonic and Terahertz Spectroscopy (HATS): Methods and Applications

Yindong Huang ^{1,2} , Chao Chang ², Jianmin Yuan ^{1,3}  and Zengxiu Zhao ^{1,*}

¹ Department of Physics, National University of Defense Technology, Changsha 410073, China; yindonghuang@nudt.edu.cn (Y.H.); jmyuan@nudt.edu.cn (J.Y.)

² National Innovation Institute of Defense Technology, AMS, Beijing 100071, China; changc@xjtu.edu.cn

³ Graduate School of China Academic of Engineering Physics, Beijing 100193, China

* Correspondence: zhaozengxiu@nudt.edu.cn

Received: 11 January 2019; Accepted: 21 February 2019; Published: 27 February 2019



Abstract: Electrons driven from atom or molecule by intense dual-color laser fields can coherently radiate high harmonics from extreme ultraviolet to soft X-ray, as well as an intense terahertz (THz) wave from millimeter to sub-millimeter wavelength. The joint measurement of high-harmonic and terahertz spectroscopy (HATS) was established and further developed as a unique tool for monitoring electron dynamics of argon from picoseconds to attoseconds and for studying the molecular structures of nitrogen. More insights on the rescattering process could be gained by correlating the fast and slow electron motions via observing and manipulating the HATS from atoms and molecules. We also propose the potential investigations of HATS of polar molecules, and solid and liquid sources.

Keywords: ultrafast intense laser; atoms and molecules; high harmonic generation; terahertz wave; electron dynamics

1. Introduction

Recent advances in attosecond science open a new era of physics for the ultrafast insight and manipulation of electrons with its natural timescale for matters in gas, liquid or solid states [1–5]. Attosecond electron dynamics are usually initiated by intense laser pulses. A bound electron of an atom can be liberated from passing over or tunneling under the binding barrier and subsequently driven by laser fields [6]. The ionization time of electron determines the subsequent actions, including the re-collision with the parent ion, roaming around the atomic core or directly escaping from the parent ion [3].

In general, the acceleration of charged particle leads to electromagnetic radiations. Under strong laser fields, re-colliding electrons could accumulate energy to recombine with the parent ions giving rise to high harmonics generation (HHG) with frequency of extreme ultraviolet (XUV) or even the soft X-ray [7,8]. Measurements of these emissions can help to understand the rescattering dynamics of electrons with high kinetic energy [9]. In a semi-classical view of HHG, different orders of high harmonics are generally determined by the ionization times of the emitter electrons. Once the ionization time is determined, the following laser fields and the electronic motion are also determined, which define a particular quantum orbit. Therefore, by analyzing the phases and the amplitudes of high harmonics, we can realize a sub-femtosecond description of the detailed interaction between the strong laser fields and the atoms within one laser cycle. Recent studies begin to pay attention to the high harmonics near or below the ionization threshold [10–12] (as well as other below-threshold phenomena, such as photoionization [13–15]), which requires a modified picture other than the simple-man model to better understand the interplay of the atomic potential and laser fields on the rescattering dynamics.

On the other side of the spectroscopy from strong field interaction, extremely nonlinear down-conversion of the laser frequency could take place via the terahertz (THz) wave generation, which has a millimeter and sub-millimeter wavelength [16]. Interestingly, the great discrepancy between HHG and THz output seems to be mainly determined by the ionization time of the emitter electrons, calling for a unified “non-perturbative” strong field viewpoint in understanding the classical “perturbative” region of laser and matter interaction. Slow electrons for THz output should be modeled differently from the ones for the plateau or cut-off of high harmonics even though they are driven by the same laser fields, because the slow electron motion could be strongly distorted by the Coulomb potential. This Coulomb field effect has been identified by tracing the phases of THz wave with the help of high harmonics [17,18], and by analyzing the underlying dynamics via classical [19] and quantum calculations [20]. Therefore, the simultaneous detection of the high-harmonic and THz spectroscopy (HATS) gives us an opportunity to illustrate more aspects of the ultrafast dynamics of electrons with different ionization times, especially for the electrons contributing to the low-energy THz wave generation.

Furthermore, the joint measurement in HATS allows the in situ simultaneous manipulations on the two ends of emissions, which could be realized by varying the accumulated phase during the electron propagation (e.g., using dual-color laser fields [17]) or varying the potential curve (e.g., varying the molecular alignment [21]). The first experimental demonstration of HATS from gaseous argon was reported in 2012 [17]. With the help of a weak second-harmonic, the symmetry of the consecutive half cycles of the fundamental laser fields is broken to produce significant intensities of the even-order high harmonics [22] and THz wave [16], whose yields depend on the relative phase between the two colors. Note that the in situ simultaneous manipulation is carried out on all electrons in the laser fields, thus it helps to build a phase-locked connection between different scales of electronic movements with various kinetic energies and collision processes. Meanwhile, the simultaneous generations and manipulations of HATS can also serve as a more convenient choice in carrying out the time-resolved THz pump/X-ray probe measurements via a table-top femtosecond laser, in comparison to the expensive and huge electron bunch setup or free electron laser light source [23–25].

Here, we review the state-of-the-art HATS technology. Firstly, we give a general introduction to the physical concept of this method. Next, we discuss two examples of HATS detection from argon. In the first example, we demonstrate the simultaneous detection of HATS from argon to study the THz generation with attosecond time resolution, thanks to the intrinsic chirp of the electron wave packet and the corresponding HHG. Particularly, HATS highlights the importance of the Coulomb potential on the rescattered electrons, as also discussed in Ref. [26] and references therein. It suggests that the strong field approximation (SFA) treatment [27–29] (as well as the SFA-based theories) may not be sufficient for dealing with the rescattered electrons, because typical SFA mainly considers the effect of the external field on the continuum state but neglects the influence of the Coulomb potential and the excited states. In the second example, we discuss that the joint measurement enables benchmarking HHG by using THz yield as a reference to calibrate the geometry phase of the driving pulse which is essential in HHG. Based on HATS, it is found that THz generation is related to the soft collision between the accelerated electrons and the ion, while HHG is related to hard collision. Therefore, it is possible to use HATS to fully characterize the electron wave packet, which is crucial in strong field physics, in particular when the driving pulse is shaping or gated.

Thirdly, we review two examples of HATS detection from molecules. It is shown that THz yields help minimize the uncertainty and assumptions of the molecular frame photoionization cross sections, which can be estimated from HHG. The phase-delay dependence of THz generation helps resolve the optimal phases of aligned nitrogen molecules to maximize the yield of even-order high harmonics.

Finally, we propose the probable extensions of the HATS method to polar molecules and other systems. We expect that HATS will be helpful in characterizing the interplay or competition between different ultrafast electronic processes in the near field regions for more complex molecules while detecting the corresponding emissions in the far field regions.

1.1. High-Order Harmonics and Terahertz Wave: Up- and Down-Conversion of Laser Frequency

The interaction between atoms or molecules and the intense laser fields induces a dipole moment that leads to the emissions of high-order harmonics, which can be considered as the up-conversion of the fundamental laser frequency. In 1992, Corkum [6] and Kulander [30] interpreted this generation process by the classical three-step model: an electron is freed from the laser dressed Coulomb field, accumulates energy E_k within the propagation and is finally driven back to the nuclei to emit photons with energy Ω equalling $E_k + I_p$. This simple man model can give an intuitive interpretation to some experimental observations, such as the cut-off energy of the harmonic spectroscopy, the long and short trajectories of electrons and the chirp between different orders of high harmonics [31]. In terms of quantum mechanics, the freed electron can be viewed as a spreading wave, and the re-collision of electron can be treated as the coherent superposition of the recombined and the remaining electronic wave packets [32]. Typically, only the odd harmonics of the fundamental laser pulses can be generated, due to the coherence between the consecutive periodic emissions. The even harmonics [22] or the supercontinuum [33,34] can also be generated by breaking the symmetry of the electric field via adding a weak second harmonic pulse.

Atoms or molecules in strong laser fields can radiate THz wave with the photon energy at meV, which is the down-conversion of the fundamental laser frequency. The first experimental observation on the far infrared/THz emissions from the interaction between laser and rare gas atoms was carried out by Hamster in 1993 [35], reflecting the pondermotive force on electrons. In 2000, Cook and his fellows developed the dual-color method to dramatically enhance the THz output [16]. Meanwhile, the dual-color relative phase dependence of THz yield is also investigated, attempting to clarify the generation mechanism [36]. There was a long-existing debate on the generation mechanism, i.e. the third-order nonlinearity parameter from the viewpoint of nonlinear optics, and the current model from the viewpoint of strong field dynamics. Cook firstly explained the enhancement of THz output by considering the third-order nonlinearity parameter $\chi^{(3)}$, corresponding to the process of $\Omega_{\text{THz}} = \{\omega_{\text{FP}} + \omega'_{\text{FP}}\} - \omega_{\text{SH}}$ and $\Omega_{\text{THz}} = \omega_{\text{SH}} - \{\omega_{\text{FP}} + \omega'_{\text{FP}}\}$. Here, the subscript indexes of frequency “FP” and “SH” indicate the photons from the fundamental laser pulses and the second harmonics, respectively. If the fundamental laser pulse is monochromic, the THz output will vanish. Otherwise, the femtosecond laser pulse shares the band width at THz frequency range (for instance, 100 fs in time domain corresponds to 10 THz in frequency domain under the Fourier transformed limit), which gives birth to the non-zero THz wave generation from the four-wave mixing mechanism. In 2004, Krell found that ionization was a prerequisite for THz generation under the dual-color fields by checking the laser intensity dependent THz output [37]. Bound electrons of atoms or molecules in air undergo tunneling ionization from strong laser fields, which occurs mostly near the laser peaks. When only the fundamental laser is present, the net current is zero summed over one laser period. However, by adding a second harmonic with a non-zero relative phase, the asymmetrical ionization from the alternating laser field leads to the nonvanishing directional current between the two consecutive half cycles. Based on the nonvanishing net current of electrons in air-plasma, Kim proposed the plasma current model [38]. This model was verified by solving the time dependent Schrödinger Equation (TDSE) of the electron dynamics within the THz emission process by Karpowicz and Zhou [39,40].

1.2. Rescattering Process and the Joint Measurement of HATS

The (plasma) current model for THz generation is analogous to the other strong field phenomena by treating the electron dynamics as the radiation source. Temporal and spatial asymmetric current could contribute to the THz generation under strong dual-color field scheme. In the sparse gas circumstance, atoms or molecules are far away from each other, thus the emissions can be treated as the coherent summation over the individual emitters. Therefore, rescattering process of the tunneling electron from one atom or molecule could be understood via analyzing the far-field THz emissions, as well as the HHG.

It is of great interest to know which part of the electron dynamics dominates the contribution of THz wave generation. Trying to reach the answer, we recall the low-energy structure (LES) of above-threshold ionization. In 2009, Blaga [13] and Quan [14] observed the appearance of the anomalous spectral peaks of photoelectrons in the low energy region. These LES peaks can be reproduced by the TDSE calculations but not by the SFA model. Faisal, who raised the SFA model, suggested the effect of the long-range Coulomb potential on the forward-rescattering of the tunneling electrons in interpreting the LES [41]. The following experiments and theoretical developments support his interpretation. By using the elliptically polarized laser to ionize electrons, which suppresses the rescattering process, LES is found to disappear [13,42]. The semi-classical calculations based on quantum orbit theory also confirm the influence of atomic potential on the rescattered electrons for the LES [43,44]. By comparing the forward-scattering from the Yukawa potential or the long-range Coulomb potential, the LES of photoelectrons is proven to be determined by the forward rescattering of electrons with the Coulomb long-range tail [45].

On the other hand, the three-dimensional classical-trajectory Monte Carlo (3D-CTMC) method and the 3D-TDSE results suggest that the low-energy photoelectrons, with the kinetic energy less than $1.2 U_p$, are responsible for the THz emissions from dual-color laser scheme [19,20]. In Kim's plasma current model, only the current formed by the freed electrons is considered as the source for THz wave generation, and the Coulomb interaction is being neglected. However, according to the observations of LES, the long-range Coulomb interaction can dominantly influence the motion of the low-energy photoelectrons. Therefore, due to the effect of the Coulomb field and the forward-rescattered electrons, the optimal phase for THz yield should be different from the one as predicted by the plasma current model. Previous calculations suggest that, under the typical laser condition (800 nm, with the laser intensity around 10^{14} W/cm²), the forward-rescattered photoelectrons with Coulomb attraction dominate the current for THz yields, resulting in the optimal phase for THz yield around 0.8π [19].

By carrying out the simultaneous detection of HATS from argon, we used the attosecond resolution of harmonic chirp to gauge the THz emissions, presenting the dual-color phase dependence of THz modulations and clarifying the importance of the forward-rescattered electrons in the THz generation process [17,18]. These experimental results suggest the importance of Coulomb interaction on the rescattered electrons and update the understanding of the generation process of THz wave. The major advantage of HATS is that it allows a simultaneous observation of the two ends of the emitted spectra from atom or molecule under strong field interaction, which correlates the fast and slow electron motions via observing and manipulating the HATS. Measuring HATS is actually the observation of different rescattered electrons during the strong field process, since the "hard" recollision electrons emit high harmonics, while the escaping and forward rescattered electrons contribute to THz generation. Therefore, the two emissions could be compared to find new results about the rescattering by monitoring different kinds of electrons (from their emissions) simultaneously. For instance, the THz wave generation, which is a quite slow process compared to the generation of high harmonics (within sub-cycle of laser), can be precisely controlled and understood by tracing the dual-color relative phase dependent yield, which can be found in Section 2.1. THz yield modulations can also be served as a robust ionization reference, which is not critically influenced by other factors such as to the phase matching condition of high harmonics.

The above depict of the rescattering process of HATS and LES is based on the time evolution of the electron wavepacket, which is building a bridge between optical emissions and the corresponding electron dynamics. Another perspective is to connect the separated pictures of the electron dynamics and the corresponding photon emission in the frequency domain, following the concept of "non-linear optics". As shown in Figure 1a, the generation of the q th harmonic can be easily understood by the up-conversion of the fundamental laser frequency. It should be noted that here the order of harmonic q should be odd, and for the even-order high harmonics, the participation of the second harmonic pulse should be considered. For instance, the q th harmonic (odd) can be combined with one photon of the fundamental pulse and one photon of the second harmonic pulse, and the output will be the $(q + 3)$ th

harmonic (even). It is tricky to use this viewpoint of energy transform for THz generation due to the failure of the four-wave mixing theory in interpreting the prerequisite of ionization [37]. However, this could be understood by many “analogous four-wave mixing channels” taking place among all the laser-dressed states, which could be written as $\Omega_{\text{THz}} = \{q \times \omega_{\text{FP}} + \omega'_{\text{FP}} + \omega''_{\text{FP}}\} - \{q \times \omega_{\text{FP}} + \omega_{\text{SH}}\}$, and $\Omega_{\text{THz}} = \{q \times \omega_{\text{FP}} + \omega_{\text{SH}}\} - \{q \times \omega_{\text{FP}} + \omega'_{\text{FP}} + \omega''_{\text{FP}}\}$ [40]. The subscript indexes of FP and SH are similar to the ones applied in Section 1.1, indicating the photons of the fundamental laser pulses and the second harmonics. Note that the THz wave output can be non-zero due to the broad bandwidth of the fundamental pulse. Typically, the second harmonic pulse is considered as a weak-field, thus only one photon with frequency ω_{SH} participates in the nonlinear process. q represents the amount of photons.

In this section, a unified physical picture for HATS and rescattering process is presented, including the emissions, the electron dynamics in time domain and the “extremely non-linear optics” in frequency domain. Based on this unified picture, the up-conversion of laser energy can be observed by the high-above threshold ionization (electron) and HHG (photon), while the down-conversion can be traced by the LES (electron) and THz wave (photon).

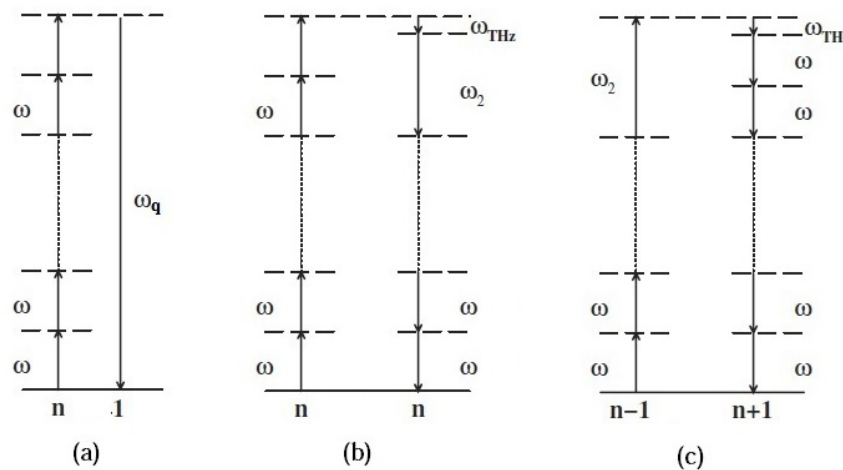


Figure 1. (a) The up-conversion of the fundamental frequency (ω) to generate the q th high harmonics ω_q ; and (b,c) the general process of the down-conversion of laser frequency (ω) to generate THz wave (ω_{THz}), with the help of the second harmonic pulse (ω_2).

2. HATS for Atoms

2.1. Attosecond-Resolved THz Generation from Argon

Typically, atoms driven by dual-color laser fields can produce few-cycle THz pulse with a pulse duration of several picoseconds. The femtosecond laser pulse determines the THz emission by the low frequency component within the laser-induced dipole of atoms or molecules. By delaying the relative phase between the two colors for about 300 attoseconds, THz output can be switched from on to off. It is surprised that the low frequency emissions could be manipulated by the sub-optical-cycle motion of electrons under the femtosecond strong laser field, which implies the existence of coherence in the electronic current.

To understand the corresponding dynamics of THz generation, a clock with attosecond resolution is required. The phases of high harmonics carry the attosecond chirp and can be treated as a clock for ultrafast dynamics [46], because different orders of high harmonics are associated with their unique recombination and emission times of the corresponding classical trajectories [47]. Generally, for atoms that have no significant structure (minimum or maximum) on the photoionization cross section, the group delay between the neighboring harmonics, also called as the “atto-chirp”, exhibits a linear dependence on the harmonic order [1,48,49]. Assuming the dual-color laser fields take the form of $A(t) = A_\omega \cos \omega t + A_{2\omega} \cos(2\omega + \phi)$, where A_ω and $A_{2\omega}$ are the fundamental and the second

harmonic electric fields with $A_{2\omega} \ll A_{\omega}$, and ϕ is the dual-color relative phase. The weak second harmonic introduces a perturbation on the propagation of the re-collision electrons [22], which can be written as

$$\Delta_{2\omega} \approx \frac{A_{\omega}A_{2\omega}}{2\omega}(\sin \omega t_r - \sin \omega t_i) \cos(2\omega t_r + \phi), \tag{1}$$

with t_i and t_r being the ionization and recombination times of electrons, respectively. The ionization time t_i determines the subsequent dynamics of the electron, resulting in different accumulated energies, i.e., the different harmonic orders. The modulations of the even harmonics are due to the perturbation of the weak second harmonic field within the electron propagation, which is proportional to $\sin^2 \Delta_{2\omega}$ [18]. Thus, based on Equation (1), the output of one even-order harmonic reaches its maximum when the dual-color relative phase ϕ_{max} equals to $-2\omega t_r$. For the adjacent odd harmonics, emission time difference is approaching 45 attoseconds under the laser intensity $3 \times 10^{14} \text{ W/cm}^2$ [50], implying that, in the case of a simultaneous HATS detection, the chirp of high harmonics provides a clock to resolve the optimal phase of THz yields with several tens of attoseconds resolution.

In 2012, Zhang and Lü reported the first HATS detection from argon, solving the longstanding debate on THz optimal phase and finding out the effect of Coulomb potential on the electron trajectory [17,18]. Dual-color fields are prepared by the Ti:Sapphire laser and its second harmonic introduced by a piece of thin β Barium Borate crystal (type I). The experimental set-up is illustrated in Figure 2a. The observed modulations of even harmonics and THz yields are fitted by $I_q \propto a_0(q) + a_1(q)\phi + a_2(q) \cos^2[\phi - \phi_0(q)]$, with a_0 the base line of modulation, a_1 the variations from the circumstance and a_2 the value of modulations from the dual-color relative phase. The experimentally determined ϕ_0 from the 18th to 24th harmonics are compared to semiclassical calculations to determine the absolute phase of the dual-color field. Using the harmonic chirp as a reference, the optimal phase for the maximum THz yield is estimated to be around 0.8π , which deviates significantly from zero as predicted by the four wave mixing model and from 0.5π as predicted from the plasma current model. Based on the plasma current model, the electron undergoes a tunneling ionization carrying no internal velocity, after which the classical movement of the ionized electrons will form a residual current to emit the THz wave. Trying to reveal the effect of Coulomb field on electron dynamics, simulations on the THz modulation were carried out and compared by applying the current model with or without the Coulomb potential.

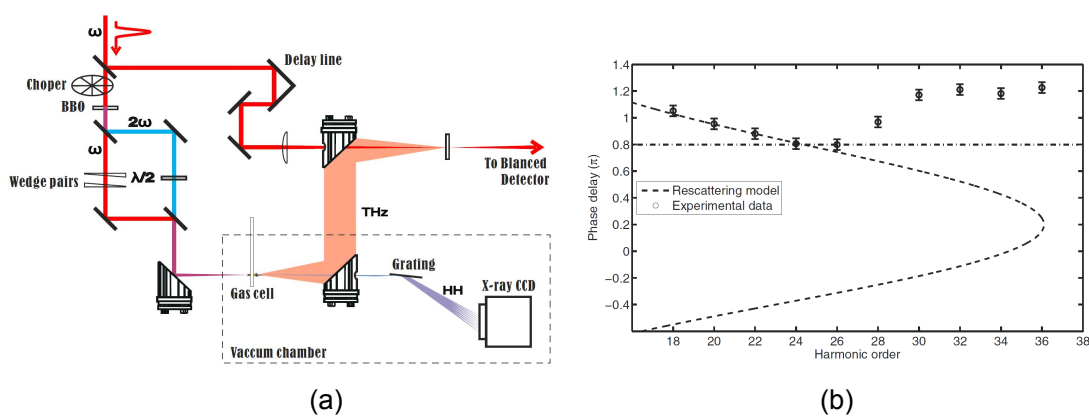


Figure 2. (a) Typical experimental set-up for HATS generation and detection. (b) The experiment obtained optimal phase for even-harmonics (circles) are compared to the semiclassical calculation (dashed line). Optimal phase for THz yield is locked at 0.8π (dotted dashed line). Reproduced with permission from [18]. Copyright IOP Publishing, 2013.

As shown in Figure 3a,b, the optimal phase for THz generation is 0.8π by analyzing the classical trajectories of the directly escaping and rescattered electrons, and this result is comparable to the

1D-TDSE calculations and the experimental observations. Meanwhile, by using the 3D-CTMC method, the current formed by the low energy electrons ($<1.2 U_p$) as a function of the dual-color relative phase exhibits a maximum at 0.72π , as illustrated in Figure 3c. Besides the classical trajectory methods, solutions on the 3D-TDSE of argon in strong laser fields also reveal a similar trend for THz yields peaking at around 0.75π when the Coulomb field is included. Based on the theoretical works on the 1D/3D classical trajectory and quantum analysis, we draw a conclusion that the escaping and rescattered electrons contribute to THz wave generation within dual-color laser field regime. These theoretical results are compared to the experimental observations to create a unified image of the rescattering events, which includes “hard collision” (recombine to the mother ions) of the rescattered electrons to emit high harmonics and the “soft collision” (forward rescattered electrons) to give birth to the THz emissions [17,18]. The most common method in modeling strong field physics is to use the SFA, which is developed by Lewenstein in 1994 [32]. In SFA, the electron in the continuum can be treated as a free particle exposing in the external electric field, with the Coulomb potential being neglected. When the electrons are far from its parent ion during the propagation step (the second one of the three steps), the Coulomb interaction between the electrons and the ions are much weaker than the interaction between laser and electrons. That is why the Coulomb interaction is neglected in the SFA model, and, for the electrons with high kinetic energy (contribute to HHG), this model typically works. However, THz generation is mostly contributed by slow electrons, which could hardly be described under the SFA model (or other models developed for high energy electrons). The dynamics of the slow electrons is also one part of the whole strong field dynamics. That is why the studies on HATS could be helpful to give more insights on the rescattering process.

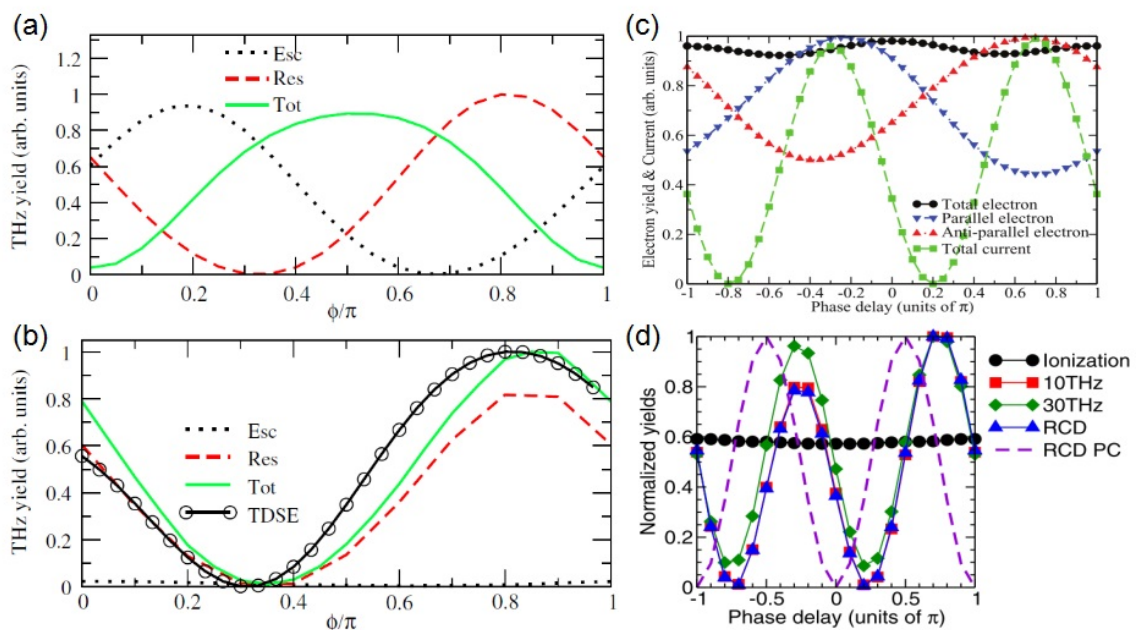


Figure 3. (a) THz yields by the escaping (black dotted line), the rescattering (red dashed line), and the total currents (green line) calculated from the plasma current model. (b) Calculated classical and 1D-TDSE results of THz yield modulation with the Coulomb interaction. (c) Current simulated by the 3D-CTMC method (green squares). (d) THz yield modulations below 10 THz (red squares), 30 THz (green diamonds) and the total residual current (blue triangles) calculated by the 3D-TDSE simulations. Reproduced with permission from [17,19,20]. Copyright APS Publishing, 2012, 2014, 2015.

In brief, the simultaneous measurement of THz wave and HHG enables the calibration of the absolute optimal phase for THz wave generation by taking advantage of the intrinsic chirp of high harmonics (the phase could also be inferred from the yield of high harmonics, as demonstrated by X. He et al. [51]). HATS is useful in determining the phase of the dual-color laser field in an all-optical

way, which is easier to carry out than measuring the photoelectrons or ions [52–54]. The measured absolute optimal phase at 0.8π has significance, which is against the predictions from previously widely-adopted four wave mixing model and (plasma) current model. Our further investigations show that the optimal phase is in fact nearly universal [20], reflecting the particular subcycle ionization dynamics in THz wave generation. The cut-off of high harmonics is mainly contributed by the electrons released at 0.17π after the peak field, while THz generation is mainly contributed by the electrons released before the peak field at -0.1π . Without Coulomb field, the latter electrons will directly escape without revisiting the atomic core. Therefore, HATS allows us for the first time to demonstrate the importance of the atomic potential in THz wave generation from atoms and molecules, which was also well known for the solid state systems (see, e.g., [55–58] and references therein). Based on HATS, we find that subcycle ionization dynamics and the following electron–atom collision, either hard collision or soft collision play important roles in the radiation from atoms driven by strong fields. By manipulating the emission process, which is a near field control and detecting in the far field, both radiation can be used to resolve the electron dynamics in attosecond resolution regardless of the 5–6 order difference of the radiation wavelength.

2.2. THz Benchmark for the Long and Short Trajectories of HHG

Typically, gas sources of high harmonics require high particle density by adiabatic expansion from a gas jet or gas cell to a vacuum chamber. The conversion efficiency of the high harmonics can be maximized via the phase-matching by adjusting the position (relative to the laser focus) and the backing pressure of the gas-supply instrument.

In 2016, Gragossian and his fellows reported the HATS detection of argon [59]. By controlling the position of the gas jet, dual-color relative phase dependent high harmonics and THz yields are studied by selecting only the short trajectory contributions, or both the short and long trajectory contributions. If the gas jet is placed at the down stream of the propagating direction, i.e., the phase-matching position, HHG from the short trajectory contribution is optimized and this results in a nearly linear relationship between the harmonic orders and the optimal phases. Under this condition, it can be found in Figure 4c that the optimal phase for the 26th harmonic coincides the phase for maximum THz yields, similar to that previously reported [17]. Note that the laser intensity of Gragossian's experiment (4×10^{14} W/cm²) is about four times larger than the early one from Zhang [17]. Since the harmonic chirp is related to the cut-off energy, the optimal phases of the 26th harmonic should be different under the two different experimental conditions. Hence, further investigations may be required to clarify whether and why THz and some specific order of HHG prefer the same dual-color phase.

If the gas jet is placed closer to the focus, as shown in Figure 4e, the long trajectory contribution dominates for the low order harmonics (less than 30), while the short trajectory chirp appears significantly at larger harmonics. Meanwhile, in the harmonic yield, as shown in Figure 4e as a function of the relative two-color phase, a complex chirp can be seen due to the coexistence of the contributions from the long and the short trajectories. Harmonic phase of the short trajectory contribution could be balanced by the Gouy phase shift, the neutral gas dispersion, the dispersion of plasma (if the ionization is significant) and the phase of the atomic dipole moment [60], to give a clear linear relationship. It is interesting to investigate the spatially and spectrally resolved quantum paths of the long and short trajectories of electrons from experiment and theory [61–65]. The joint measurement of HATS is a supplementary to these results, which can use THz wave generation as a phase reference for the long and short trajectories of electrons. Especially for the dual-color laser generation case, the propagation of electron can be manipulated by the weak second harmonic, resulting in the simultaneous manipulation of the long and short trajectory with THz emission as a reference.

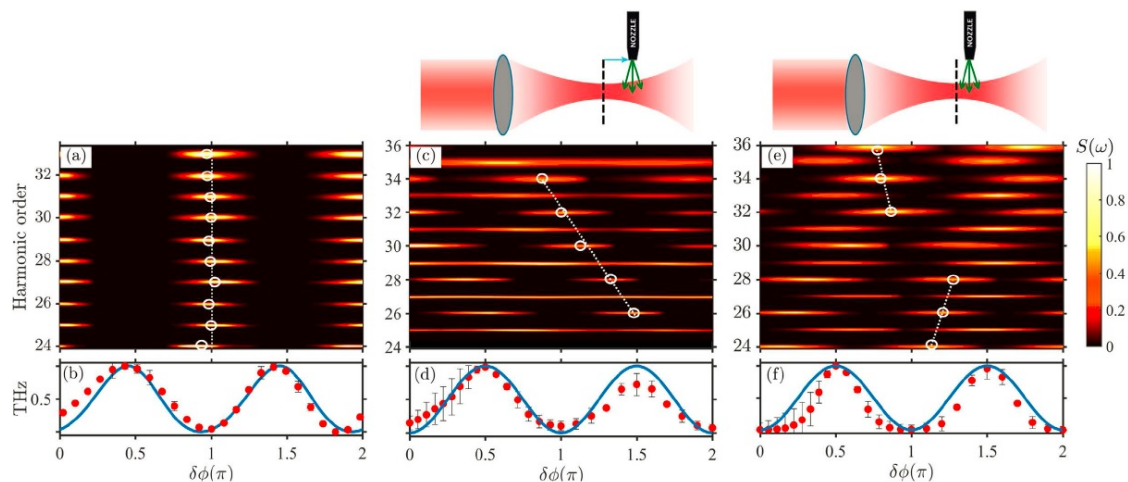


Figure 4. The modulations of high harmonics and THz yields with strong second harmonic (intensity ratio about $A_2^2/A_1^2 = 0.1$ (a,b)) and weak second harmonic ($A_2^2/A_1^2 = 0.005$) (c–f). The laser condition of (c,d) is for phase-matching condition of the gas jet, while the gas jet is positioned closer to the focus of the laser in (e,f). Reproduced with permission from [59]. Copyright Springer Nature Publishing, 2016.

If the driving laser has a cosine time-dependent shape, the last quarter period of electron dynamics could be traced by the long trajectory of the recombined electrons [66]. As demonstrated in Refs. [62,65], simultaneous observation and manipulation on the long and short trajectory of electrons could serve as a supplement to the typical high harmonic detection with only the short trajectory contributions. We suggest a combined detection of both the short and long trajectories as well as the dual-color controlled HATS modulations to give deeper insights into on the dynamics of electrons in strong laser fields.

When the intensity of the second harmonic is no more a perturbation, which occurs for example at about 0.1 of the intensity of the fundamental field, modulations exhibit an out-of-phase relationship between the yields of THz and different harmonics, as illustrated in Figure 4a,b. This could be understood within the schema of the classical three-step process. For strong second harmonic laser field condition, the modulations of even harmonics no longer originate from the perturbation action of the electron trajectories. Intuitively, recombined electrons dominate the emission of high harmonics, thus the amount of the escaping and forward-rescattered electrons decreases, leading to the reduction of the electronic current for THz generation. As shown in Figure 5a and discussed in Ref. [67], the phase for the maximal THz intensity varies when the gas jet is positioned around the laser focus. Here, each subplot in Figure 5a labeled by the position of the gas jet is normalized to its absolute value of the maximal THz amplitude under this specific gas jet position. Each spectrum along the horizontal direction within each subplot indicates the THz waveforms under different relative phases of the dual-color field when the gas jet is placed at the specific position relative to the laser focus. The dual-color phase dependent THz yields allow the reconstruction of the Gouy phase, which comes from the propagation of the focusing laser [68]. The Gouy phase shift also has an influence on the optimal phases of HHG, which can be found in Figure 5b–d. Note that the relative phase in Figure 5 does not correspond to the value of the absolute phase between the fundamental and the second harmonic pulse, while the absolute phase could be determined by the optimal phases of HATS (as demonstrated in Section 2.1).

There exist two advantages in detecting the long and short trajectories of the electrons from HATS. On the one hand, the phase shift caused by the focusing of laser, such as the Gouy phase shift, could be eliminated straightforward when comparing to the dual-color relative phase dependent HATS, as illustrated in Figure 4c,e. On the other hand, dynamics of electrons contributing to the long and short trajectories for HHG could be revealed by the phase reference provided by the THz modulation, because the classical trajectories can be mainly categorized according to their ionization times.

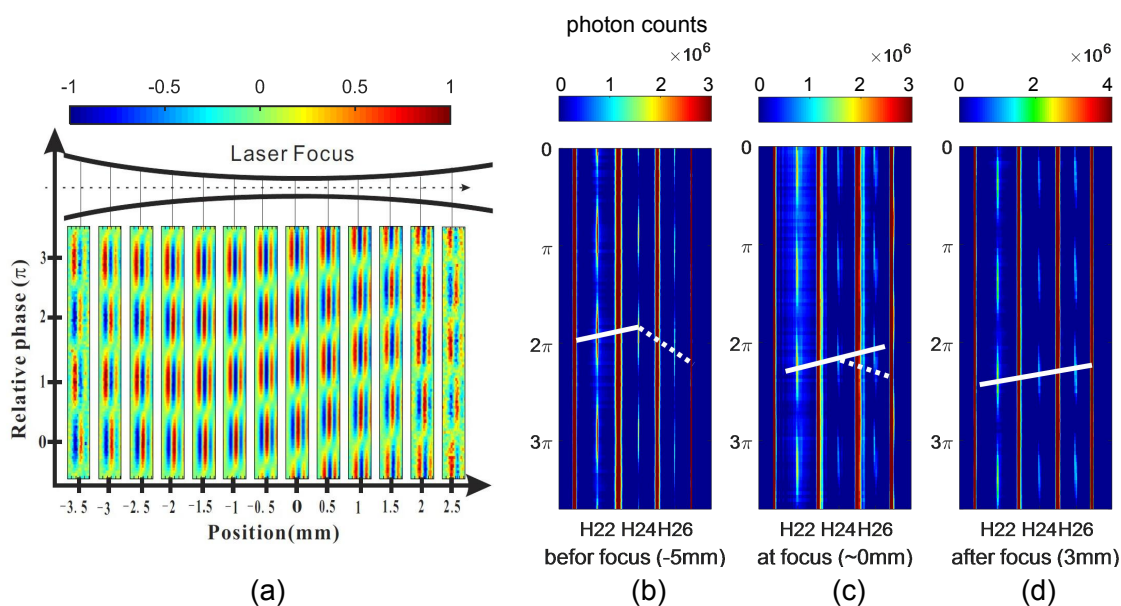


Figure 5. (a) Normalized THz waveform as a function of the dual-color relative phase and the position of gas jet. (b–d) The harmonic yields (with the background signals removed) as functions of the dual-color relative phase and the position of gas jet relevant to the laser focus. For a clear visualization of the intensity modulations of the even harmonics, the intensity at and beyond 3×10^6 photon counts is represented by the same color scale. The solid (dashed) white lines indicate the short (long) trajectory contributions.

3. HATS for Molecules

3.1. THz Reference for Molecular Photoionization

In this section, we introduce two examples of HATS applications for molecules. In general, the arbitrary pointing direction of a molecule obstructs the direct observation of the angular structures of molecular orbital. Thanks to the development of molecular non-adiabatic alignment techniques [69], tomography of the highest occupied molecular orbital (HOMO) was demonstrated on nitrogen molecule in 2004 [70]. Since then, high harmonics from aligned molecules are applied to image the HOMO of carbon dioxide [71,72], the lower occupied molecular orbitals of nitrogen [46,73] and carbon dioxide [49,74,75].

Based on the quantitative re-scattering (QRS) model on HHG, alignment-dependent HHG from molecules can be viewed as the product of the alignment-dependent ionization rates and the recombination matrix elements, while the recombination of electron and the subsequent emissions of the harmonics is the inverse process of photoionization [76]. Therefore, high harmonics from aligned molecules can be applied to deduce the molecular photoionization cross section (PICS). However, previous research required the separated calculation or experiment on the angle-dependent ionization of molecules. On the one hand, the ionization theories of molecules predict the wrong angular dependence when comparing to the experimental observations, such as the molecular strong field approximation (MO-SFA) [77] and the molecular Ammosov–Delone–Krainov (MO-ADK) theory [78]. For nitrogen or oxygen, there is only discrepancy in the absolute size of the angle-dependent ionization rates, while, for carbon dioxide, the calculated angle of peak ionization appears at around 30 degrees aligned angle between the molecular axis and the driven laser field polarization, but experimental results support the 45-degree alignment [79,80]. On the other hand, the source density for harmonic emission is about 10^{17} cm^{-3} , which is below the typical detection limit of electrons or ions. This low density makes the joint measurement on high harmonics and electrons/ions from aligned molecules a challenging task.

Instead, THz wave generation from aligned molecules can be treated as a calibration of the angular dependent ionization. According to the rescattering process discussed in Section 2.1, THz generation is mainly caused by the directly escaping and the forward-rescattered electrons. This makes the alignment dependent THz yield a suitable benchmark to calibrate the angular dependent ionization of molecules. Alignment dependent THz yield of molecules is proportional to the square of angular ionization probabilities [81]. Thus, by carrying out the joint detection of HATS from aligned molecules and using the alignment dependent THz yields, the angular differential PICS could be retrieved [21,82].

The light path for HATS measurement on molecules is analogous to the one in Figure 2a, with an additional beam for molecular alignment [21]. As shown in Figure 6, normalized modulations of HATS are compared under different alignments. Note that the modulations are obtained from the aligned yields subtracted by the random aligned yields, and then normalized to the maximum value for the 21st harmonic and THz wave, respectively. There is a positive correlation between the THz generation and the 21st harmonic generation from nitrogen. It has been reported that there also exists a positive correlation between the 23rd harmonic and the ions output of nitrogen [71], and the pump–probe delay dependences of the harmonic yields from the 21st to 25th orders show similar structures [83]. Therefore, since the pump–probe delay dependent modulations of the 21st harmonic and the THz yields are positively correlated in Figure 6, we can conclude that there exists a positive correlation between THz yields and ionization yields of N_2 . The alignment dependent THz result from Y. You et al. is also consistent with this conclusion by analyzing the THz yields from laser-aligned air [81]. More interestingly, when the aligned laser is linearly polarized at 50 degrees of the alignment angle, the magnitude of the modulation of high harmonic decreases significantly. This specific angle is called as the “magic angle”, indicating the combined effect of the evolution of the rotating wavepacket and the angular harmonic yields [84].

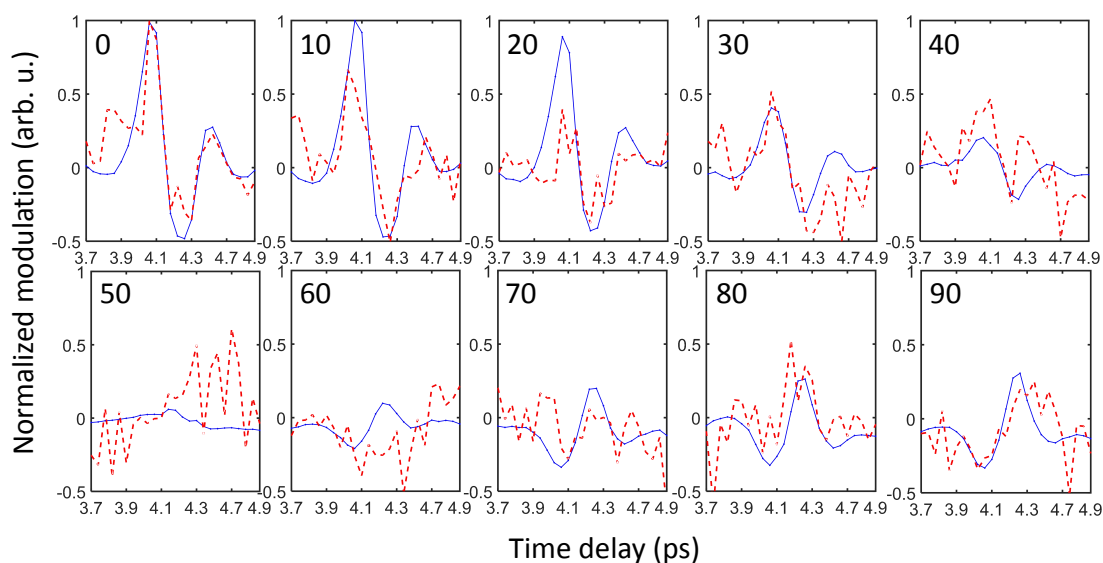


Figure 6. The modulations of the relative yields of the 21st harmonic (the blue solid lines) and the THz (the red dashed lines) as functions of the time delay between aligning and generation pulses with different aligned angles. The alignment angle is indicated in degrees at the top left corner of each subplot.

HATS method provides an all-optical way in understanding the whole rescattering process from molecules, avoiding an additional ionization experiment. The measured HATS from aligned molecules is the coherent sum of the molecular frame angular emission yields S with a distribution of rotational wave packet ρ [85,86]. It is hard to carry out coherent deconvolution to obtain the single molecular response from the experimental results, which requires the fitting on both the amplitudes and the

phases. Therefore, the incoherent summation method is used instead for the small molecules, such as nitrogen and oxygen. By comparing the differences introduced by the coherently and incoherently summation, the validity of the incoherent method was examined for nitrogen [82,87]. The incoherent sum M of the molecular frame angular yields from all solid angles takes the form of [86]

$$M(\alpha'; t_D) \propto \int_0^{2\pi} d\varphi' \int_0^\pi d\theta' S(\theta, \varphi) \times \rho(\theta', \varphi'; t_D) \sin \theta', \quad (2)$$

where θ' (φ') is the polar (azimuthal) angle about the polarization axis of the aligning pulse, $\theta(\varphi)$ is the corresponding angle in molecule frame, α' represents the angle between the polarization directions of the aligning and the generation pulses, $S(\theta, \varphi)$ is the angular yields of HATS in the molecular frame and $\rho(\theta', \varphi'; t_D)$ is the angular distribution of the rational wave packet at t_D . Note that the primed and unprimed notations of the physical quantities indicate the laboratory frame and molecule frame, respectively. Since the coordinate axis could be transformed from the molecular frame to the laboratory frame [79], the angular yields $S(\theta, \varphi)$ could be rewritten as $S(\theta', \varphi', \alpha')$. By using the incoherent deconvolution method, the experimental results and the fittings of the 21st harmonic are shown in Figure 7b,c, respectively.

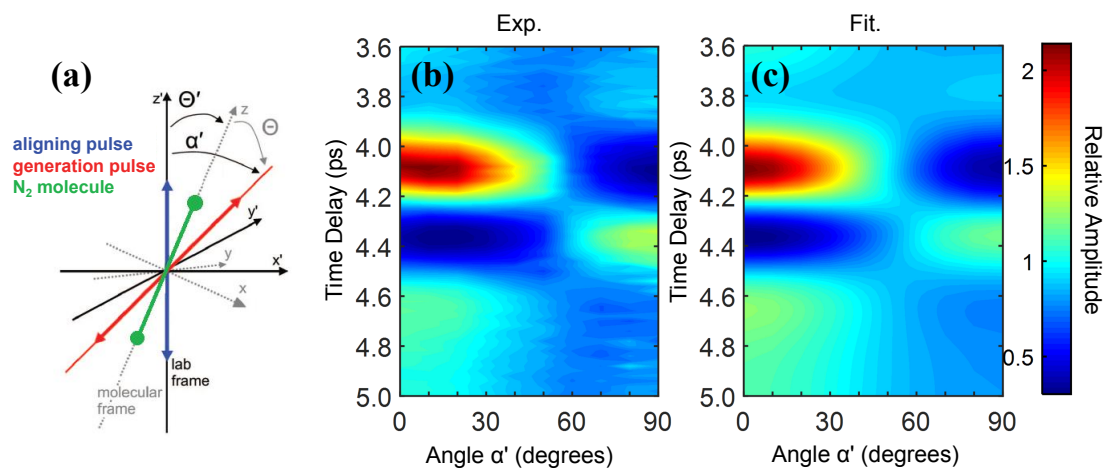


Figure 7. The reconstruction of the single molecular response: (a) the polar and azimuthal angles about the polarization axis of the aligning and the generation pulses, as well as the corresponding coordinate transformation; and (b,c) the experimental results and fittings of the relative amplitudes of the 21st harmonic (the aligned yields divided by the random pointing yields), which are functions of the aligned angles (α') and the time delay between the aligning and the generation pulses.

The alignment-dependent high harmonic yields in molecular frame $S_{\text{HHG}}(\Omega, \theta)$ can be expressed by using the QRS theory [76,88]

$$S_{\text{HHG}}(\Omega, \theta) \propto \Omega^4 W^2(\Omega) \sigma_{\text{PICS}}(\Omega, \theta) N(\theta), \quad (3)$$

where Ω is the harmonic frequency, $W(\Omega)$ is the amplitude of the flux of the returning electrons, $\sigma_{\text{PICS}}(\Omega, \theta)$ is the differential photoionization cross section of energy $\hbar\Omega$ under angle θ , and $N(\theta)$ is the angular ionization probability.

For the THz wave generated from the laser-aligned molecules, the alignment dependent THz amplitude is proportional to the cycle-averaged electric current density $J_R(\theta, t)$ [38,81,89],

$$E_{\text{THz}}(\theta) \propto \frac{d\langle J_R(\theta, t) \rangle}{dt} = \langle ev_d(t)n(\theta, t) \rangle, \quad (4)$$

where $v_d(\theta)$ represents the drift velocity of the electron released at t , and $n(\theta, t)$ is the angle-dependent ionization rates at t . It should be noted that the cycle average of $n(\theta, t)$ is proportional to the angle-dependent ionization probability $N(\theta)$.

By replacing $N(\theta)$ with the alignment dependent amplitude $E_{\text{THz}}(\theta)$, the angle-dependent differential PICS can be written in the form of [82]

$$\sigma_{\text{PICS}}(\Omega, \theta) \propto \frac{S_{\text{HHG}}(\Omega, \theta)}{\sqrt{S_{\text{THz}}(\theta)}}. \quad (5)$$

Since alignment dependent yields of HATS are obtained simultaneously, the angle-dependent differential PICS can be tracked within one run of experiment in an all-optical way. For comparison, the angle-dependent differential PICSs obtained from the HATS detection are presented with the calculation results in Figure 8. When gradually increasing the momentum of the returning electrons from the 21st to the 25th harmonics, the corresponding minimum angles of PICS also increase (green arrows), which is caused by the antisymmetric p_z orbital participation within the HOMO of nitrogen molecule [90]. The experimental [21] and theoretical [88] angle-resolved PICSs are in good agreement, indicating a promising potential application in revealing molecular structures.

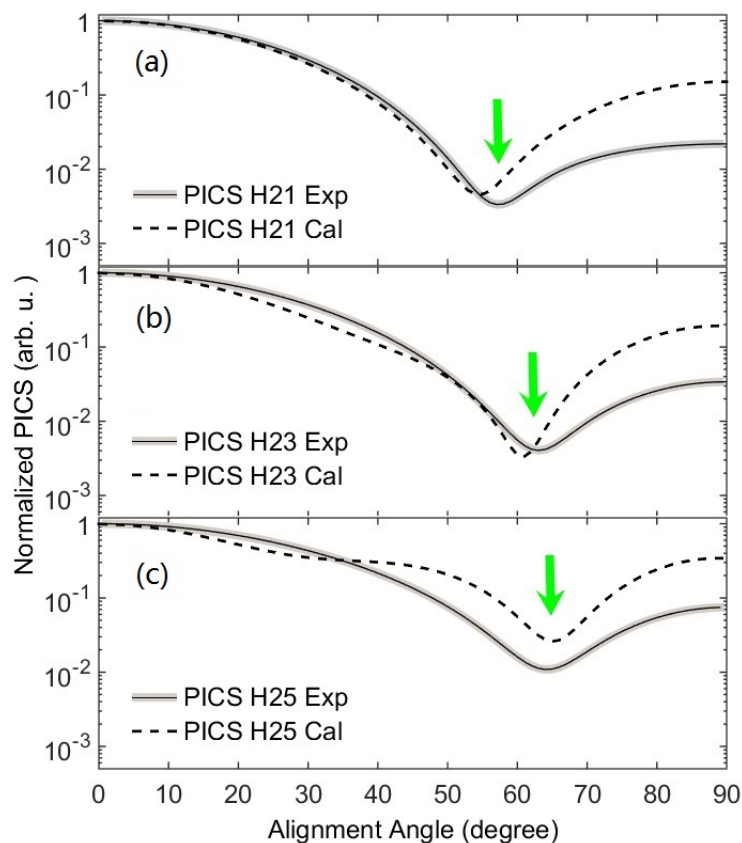


Figure 8. The normalized theoretical (dashed line) and experimental (solid line) angle-dependent differential PICS of the 21st (a), 23rd (b), and 25th (c) harmonic orders as functions of alignment. The green arrows indicate the angular minima for clarity. Reproduced with permission from [21]. Copyright APS Publishing, 2015.

3.2. The Alignment Dependent Electron Dynamics for HHG with THz Phase Reference

Phases for high harmonics are of importance in understanding the electron dynamics and compressing the attosecond pulse (train). The techniques for characterizing the harmonics' phases can be generally classified as *ex situ*, where the attosecond pulse train photoionizes a target medium with

an additional fundamental laser pulse, and in situ, where the measurement of phase takes place in the medium in which the high harmonics are generated. These two approaches form a temporal gating of detection or generation of high harmonics with an additional pulse, which are extensively reviewed in Ref. [9].

The ex situ and in situ approaches have been proven equivalent in most cases for atoms [47], but the in situ approach seems to show less dependence on the recombination phase [91]. For molecules, ex situ detections on harmonics' phases have been carried out by applying the reconstruction of attosecond beating by interference of two-photon transition (RABBIT) technique [46,49] or generating another high harmonic beam to form a Young's type two-emitter interferometer [72]. Actually, both the ex situ and the in situ approaches measure the derivative of the harmonic phase, not exactly the phase itself [1]. This raises two problems before comparing the experimental results to the theoretical calculations: (1) the absolute phases of different harmonics cannot be directly obtained from measurements; and (2) the absolute phases of high harmonics from molecules cannot be determined under different alignments. Therefore, several assumptions should be made in advance to give a phase reference, for instance, the same values of the optimal phases of the 15th harmonic from Kr and aligned CO₂ [49], the same values of the optimal phases of the 15th harmonic under all alignments of N₂ and laser intensities [46]. Applying an additional pulse to form an interferometer is a more direct way to obtain both the amplitudes and phases of high harmonics from aligned molecules [72], but it requires a quite precise control on the temporal and spatial overlapping of high harmonics from two separated emission sources [92]. Since the dual-color laser scheme could be applied as the in situ approach, these two problems can be solved easily by carrying out the HATS detection with the THz phase reference.

Firstly, it is necessary to verify the robustness and validity of the THz phase reference when applying the HATS measurements. Hard-collision electrons contribute to high harmonics could be compared with the soft-collision electrons for THz generation, because these emissions are originating from the same driving laser fields but with different birth times of the ionized electrons. Based on this fact, dual-color relative phase dependent THz modulations could serve as a phase reference to calibrate high harmonics, as demonstrated in Section 2.2. Motions of electrons can be viewed as propagation in a combined field of the Coulomb field and the oscillating laser, therefore the robustness and validity of this THz phase reference should be examined by varying the Coulomb potential and the laser fields, respectively.

To show the Coulomb potential dependence on the optimal phases, different gas types are compared in Figure 9. The results defy intuition that the optimal phases for THz output from atoms or small molecules keep nearly unchanged. Meanwhile, experiments on random, aligned and anti-aligned nitrogen molecules show nearly no difference on the optimal phases for THz output [82]. As discussed in Section 2.1, laser-controlled motion of slow electrons for THz emission can be strongly distorted by the Coulomb potential in the forward-rescattering process, but it seems counter-intuitive that this distortion exhibits scarcely any dependence on the specific Coulomb fields from different gas types or the molecular alignments. If the two-color fields are linearly polarized, the electronic motion is mainly along the direction of laser polarization (with the transverse momentum distribution being neglected). When varying the Coulomb potential, the forward-rescattered electrons should be affected as observed by the holography of photoelectrons [93,94]. However, the experimental results in Figure 9 and Ref. [82] exhibit a trivial dependence on Coulomb potential. It should be noted that the trivial dependence here does not mean the Coulomb potential is not important, but means the difference of the optimal phases between different atoms or molecules is not significant. The possible reason for the trivial dependence on gas types or molecular alignments could be attributed to the less spatial resolution of the slow electrons for THz emissions because the de Broglie wavelength of electron with 1 THz kinetic energy is about 220 Å, which is much larger than the typical size of atoms or molecules.

To examine the laser field dependence of the optimal phases of THz yield, the laser intensity of the fundamental pulse (ranging from 0.8×10^{14} to 1.8×10^{14} W/cm²) and the intensity ratios

between the second harmonic and the fundamental pulse (ranging from 0.001 to 0.1) are varied [67]. The nearly unchanged value of the optimal phases indicates that the THz optimal phase is a robust phase reference for the laser fields. Note that here the laser intensity variation is limited to make sure that the tunneling ionization still dominates the ionization of electrons. Therefore, under the typical experimental conditions for THz generation from the dual-color laser fields, the optimal phase of the slow electron for THz emission will not change under different Coulomb potential or laser conditions, which makes the modulation of THz yield a well-defined reference for the dual-color relative phase.

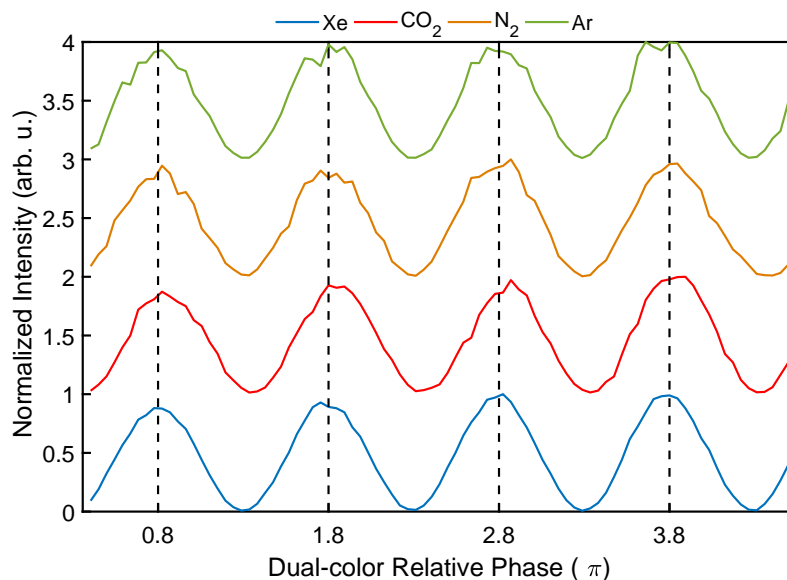


Figure 9. The normalized THz yields as functions of the dual-color relative phase for xenon (blue), carbon dioxide (red), nitrogen (orange) and argon (green) under the same experimental conditions (laser intensity of the ω and 2ω is about 1.8×10^{14} W/cm² and 1.8×10^{13} W/cm², respectively). The optimal phases for THz outputs are highlighted by the black dashed lines. Vertical shifts are applied on the baselines of different gas types to offer a more clear version.

Furthermore, HATS can help to investigate the participation of inner molecular orbital for HHG from the aligned N₂ by applying the THz phase reference. As illustrated in Figure 10, THz yield modulations exhibit no significant dependence on the molecular alignment, making the THz optimal phase a straightforward phase reference for different harmonics. By varying the aligned angle Θ and the dual-color relative phase, two-dimensional modulations of even harmonics from the 28th to the 32nd harmonics can be traced with the THz phase reference. To give a better visualization of the relative phase dependence, the modulations of each horizontal lines are normalized to their maxima. For instance, the top horizontal line of the 28th harmonic yields is normalized to the maximum value of the 28th harmonic under different dual-color relative phases with the parallel alignment. Optimal phases for the 28th and the 30th harmonics are almost the same at different aligned angles. However, for the 32nd harmonic, the optimal phases varies about 0.2π from parallel to perpendicular alignment. The modulation of the 32nd harmonic is not as clear as the modulations of the other harmonics, due to its proximity to the cutoff and its low intensity. The difference between optimal phases for different alignments could be interpreted as the participation of the lower-lying molecular orbital (i.e., the HOMO-1) at the cut off region of high harmonic spectrum. The HOMO and HOMO-1 of N₂ exhibit the σ_g and π_u symmetries, respectively. Therefore, if the polarization of the driving laser is parallel to the molecular axis, a strong dipole will be induced in the HOMO, whereas no dipole is induced in the HOMO-1. If the driving laser is polarized perpendicular to the molecular axis, the dipole for the HOMO will be weakened, whereas the HOMO-1 induced dipole will be strengthened [73]. For harmonics at the cut off region, the HOMO-1 contribution may

be strong especially when the N_2 molecule is aligned perpendicular to the generation laser pulses. This may be the reason for the alignment dependent optimal phases for the 32nd harmonic. Meanwhile, the optimal phases of THz yield can be determined as 0.8π due to the previous experiments on argon and nitrogen [17,82]. With the help of this THz phase reference, the optimal phases for different harmonics could be compared to the theoretical results directly. Nitrogen is not the only molecule for multi-orbital effect and another case could be found on carbon dioxide by applying the HATS method [95,96], which also exhibits the participation of the lower-lying molecular orbitals within the harmonic emission process [72].

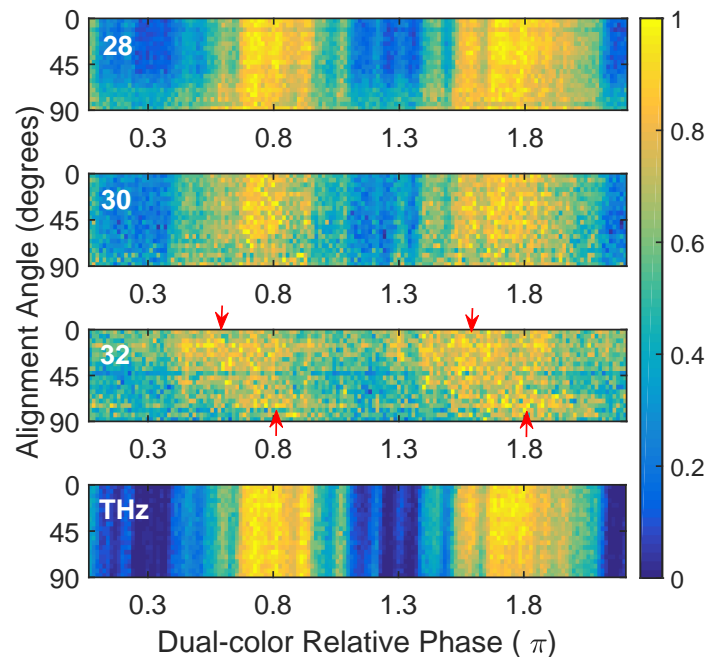


Figure 10. The normalized yield of even harmonics from H28 to H32 as a function of the aligned angle Θ and the dual-color relative phases with the THz phase reference for nitrogen. Experimental data are normalized under each alignment of different harmonics and THz wave, respectively. The red arrows help to find the phase variations of H32 from N_2 between the parallel and perpendicular alignments.

In brief, the combined measurement of HATS from aligned nitrogen reveals the absolute optimal phases with the help of the THz reference, which would be hardly accessible with HHG or THz spectroscopy alone. It may be sufficient to detect the harmonics' relative phases by applying the ex situ measurements. However, the absolute phase of high harmonics matters for compression of attosecond pulse (train) [97], for which the in situ HATS approach could provide valuable information.

4. Prospective

4.1. HATS for Polar Molecules

The detection of HATS from gas has focused on atoms or non-polar molecules with relatively simple structure and high degree of symmetry. However, in nature, many molecules exhibit polarity, which makes a well-defined orientation a prerequisite to study their angle-dependent property. Due to the inherent dipole moment, polar molecules are indeed the next potential targets for HATS detection to investigate electron dynamics under strong laser fields.

The first concern is the effect of the inherent dipole moment on the emissions. The inherent dipole moment of the polar molecule is predicted to introduce even harmonics under the interaction with the fundamental laser solely, which is different from the typical dual-color scheme of adding a weak second harmonic [98]. For the dual-color method, the symmetric motion of electrons is broken during

the consecutive two half cycles of the laser field when a suitable dual-color relative phase is applied, producing significant intensities of the even-order high harmonics and THz emissions. Therefore, even harmonics are closely associated with the emission of THz wave when they are generated by the common asymmetric electron dynamics, which underlies the HATS detection. The ionization rates of polar molecules under different orientations are mainly determined by the spatial distribution of the electronic wave function, which introduces additional asymmetry for the electrons released in the directions parallel and anti-parallel to the dipole. Therefore, even only with a single color fundamental laser, the oriented polar molecules can still generate the HATS [99,100]. Based on the discussions in Section 3.1, the orientation dependent THz yields can also be applied to detect the angle-dependent ionization of the polar molecules, or to reconstruct the angle-dependent differential PICS.

The second concern is the asymmetric Coulomb potential of polar molecules. The rescattering dynamics of polar molecules has been shown theoretically to be different substantially from that of homonuclear molecules, as reported in Refs. [101,102]. With the help of HATS technique, the asymmetry of nuclei attraction and the electron dynamics on THz wave and high harmonics may be identified, allowing more insights into the electron localization of polar molecules. The understanding of polar molecules can also help push HATS into more complex matter, such as the polymer, cluster and even the crystal.

4.2. HATS for Solid and Liquid Media

Recently, attention has been drawn to the strong field physics of matter in the solid and liquid states, which might be more efficient emission sources. Rapid developments have been made on both the technology and the understanding of the related physics [103–110]. The methods developed for gas targets can also be applied to solid by borrowing the similar physical concepts and varying from the nuclei-electron re-collision to the hole-electron re-collision [109]. This implies the possibility of generalizing the HATS technique for solids, since HATS is rooted in the non-perturbative electron dynamics driven by the strong laser field. Intuitively, the periodic potential for the ideal crystalline solid can be described by the linear combination of the atomic orbitals (LCAO), which shares a similar way of treating the molecular orbitals in quantum chemistry [111]. At present, there exist two mechanisms of the generation process of high harmonics from solid, namely the interband and intraband transitions [104,112]. Recent observations on harmonic plateaus and cut-off law also suggest new pictures of the underlying electron dynamics [107,113–116]. It is expected that the HATS for crystalline solid can be applied to clarify the motion of electrons, because the detection of THz wave, which is formed by the shifting current, may be a much more direct way to trace the electronic movements than high harmonics. Furthermore, the phonon of crystal is located within the THz frequency range [58], implying that both the electronic motions and the phonon properties can be observed within one run of detection by using our HATS method.

It is also of great interest to detect HATS from liquid source, especially on water, because water is the most common solution to matters with strong absorption of THz wave. Both HHG and THz wave have been observed from liquid water successfully: HHG was investigated by the droplets of water and THz wave was generated from thin water film [4,110]. In 1995, Thrane started the detection of THz reflecting spectroscopy from water [117]. The interactions among alkalis, alkaline-earth ions and water molecules exhibited a specific order, which was understood by the solution dynamics [118]. If HATS detection were applied to the water solution, the orientation and re-direction of the water molecules might be traced on a subfemtosecond timescale. Another interesting topic is the hydrogen bond of liquid. For instance, the interaction between the two molecules within one water dimer (H_2O)₂, is much stronger than the Van der Waals force, which implies the existence of hydrogen bond with the typical energy at THz frequency range [119]. By applying the HATS method to study the ultrafast processes in water, the hydrogen dynamics are expected to be revealed.

Funding: This research was funded by the Major Research plan of NSF of China (Grant No. 91850201) and the National Natural Science Foundation of China (Grant Nos. 11804388, 11622542, and 51677145).

Conflicts of Interest: The authors declare no conflict of interest.

Abbreviations

The following abbreviations are used in this manuscript:

THz	Terahertz
HHG	High-order Harmonic Generation
HATS	High-harmonic And Terahertz Spectroscopy
PICS	Photo-Ionization Cross Section
TDSE	Time-Dependent Schrödinger Equation
CTMC	Classical-Trajectory Monte Carlo
LES	Low Energy Structure
SFA	Strong Field Approximation
QRS	Quantitative Re-Scattering
HOMO	Highest Occupied Molecular Orbital
MO-SFA	MOlecular Strong Field Approximation

References

- Paul, P.M.; Toma, E.S.; Breger, P.; Mullot, G.; Augé, F.; Balcou, P.; Muller, H.G.; Agostini, P. Observation of a rain of Attosecond Pulses from High Harmonic Generation. *Science* **2001**, *292*, 1689–1692. [[CrossRef](#)] [[PubMed](#)]
- Corkum, P.B.; Krausz, F. Attosecond science. *Nat. Phys.* **2007**, *3*, 381–387. [[CrossRef](#)]
- Krausz, F.; Ivanov, M. Attosecond physics. *Rev. Mod. Phys.* **2009**, *81*, 163–234. [[CrossRef](#)]
- Jordan, I.; Jain, A.; Gaumnitz, T.; Ma, J.; Wörner, H.J. Photoelectron spectrometer for liquid and gas-phase attosecond spectroscopy with field-free and magnetic bottle operation modes. *Rev. Sci. Instrum.* **2018**, *89*, 053103. [[CrossRef](#)] [[PubMed](#)]
- Kruchinin, S.Y.; Krausz, F.; Yakovlev, V.S. Colloquium: Strong-field phenomena in periodic systems. *Rev. Mod. Phys.* **2018**, *90*, 021002. [[CrossRef](#)]
- Corkum, P.B. Plasma perspective on strong field multiphoton ionization. *Phys. Rev. Lett.* **1993**, *71*, 1994–1997. [[CrossRef](#)] [[PubMed](#)]
- Popmintchev, T.; Chen, M.C.; Popmintchev, D.; Arpin, P.; Brown, S.; Ališauskas, S.; Andriukaitis, G.; Balčiunas, T.; Mücke, O.D.; Pugzlys, A.; et al. Bright Coherent Ultrahigh Harmonics in the keV X-ray Regime from Mid-Infrared Femtosecond Lasers. *Science* **2012**, *336*, 1287–1291. [[CrossRef](#)] [[PubMed](#)]
- Popmintchev, D.; Hernández-García, C.; Dollar, F.; Mancuso, C.; Pérez-Hernández, J.A.; Chen, M.C.; Hankla, A.; Gao, X.; Shim, B.; Gaeta, A.L.; et al. Ultraviolet surprise: Efficient soft x-ray high-harmonic generation in multiply ionized plasmas. *Science* **2015**, *350*, 1225–1231. [[CrossRef](#)] [[PubMed](#)]
- Kim, K.T.; Villeneuve, D.M.; Corkum, P.B. Manipulating quantum paths for novel attosecond measurement methods. *Nat. Photonics* **2014**, *8*, 187–194. [[CrossRef](#)]
- Yost, D.C.; Schibli, T.R.; Ye, J.; Tate, J.L.; Hostetter, J.; Gaarde, M.B.; Schafer, K.J. Vacuum-ultraviolet frequency combs from below-threshold harmonics. *Nat. Phys.* **2009**, *5*, 815–820. [[CrossRef](#)]
- Power, E.P.; March, A.M.; Catoire, F.; Sistrunk, E.; Krushelnick, K.; Agostini, P.; Dimauro, L.F. XFROG phase measurement of threshold harmonics in a Keldysh-scaled system. *Nat. Photonics* **2010**, *4*, 352–356. [[CrossRef](#)]
- Soifer, H.; Botheron, P.; Shafir, D.; Diner, A.; Raz, O.; Bruner, B.D.; Mairesse, Y.; Pons, B.; Dudovich, N. Near-Threshold High-Order Harmonic Spectroscopy with Aligned Molecules. *Phys. Rev. Lett.* **2010**, *105*, 143904. [[CrossRef](#)] [[PubMed](#)]
- Blaga, C.I.; Catoire, F.; Colosimo, P.; Paulus, G.G.; Muller, H.G.; Agostini, P.; Dimauro, L.F. Strong-field photoionization revisited. *Nat. Phys.* **2009**, *5*, 335–338. [[CrossRef](#)]
- Quan, W.; Lin, Z.; Wu, M.; Kang, H.; Liu, H.; Liu, X.; Chen, J.; Liu, J.; He, X.T.; Chen, S.G. Classical Aspects in Above-Threshold Ionization with a Midinfrared Strong Laser Field. *Phys. Rev. Lett.* **2009**, *103*, 093001. [[CrossRef](#)] [[PubMed](#)]
- Liu, C.; Hatsagortsyan, K.Z. Origin of Unexpected Low Energy Structure in Photoelectron Spectra Induced by Midinfrared Strong Laser Fields. *Phys. Rev. Lett.* **2010**, *105*, 113003. [[CrossRef](#)] [[PubMed](#)]

16. Cook, D.J.; Hochstrasser, R.M. Intense terahertz pulses by four-wave rectification in air. *Opt. Lett.* **2000**, *25*, 1210–1212. [[CrossRef](#)] [[PubMed](#)]
17. Zhang, D.; Lü, Z.; Meng, C.; Du, X.; Zhou, Z.; Zhao, Z.; Yuan, J. Synchronizing Terahertz Wave Generation with Attosecond Bursts. *Phys. Rev. Lett.* **2012**, *109*, 243002. [[CrossRef](#)] [[PubMed](#)]
18. Lü, Z.; Zhang, D.; Meng, C.; Du, X.; Zhou, Z.; Huang, Y.; Zhao, Z.; Yuan, J. Attosecond synchronization of terahertz wave and high-harmonics. *J. Phys. B Atom. Mol. Opt. Phys.* **2013**, *46*, 155602. [[CrossRef](#)]
19. Liu, J.; Chen, W.; Zhang, B.; Zhao, J.; Wu, J.; Yuan, J.; Zhao, Z. Trajectory-based analysis of low-energy electrons and photocurrents generated in strong-field ionization. *Phys. Rev. A* **2014**, *90*, 063420. [[CrossRef](#)]
20. Chen, W.; Huang, Y.; Meng, C.; Liu, J.; Zhou, Z.; Zhang, D.; Yuan, J.; Zhao, Z. Theoretical study of terahertz generation from atoms and aligned molecules driven by two-color laser fields. *Phys. Rev. A* **2015**, *92*, 033410. [[CrossRef](#)]
21. Huang, Y.; Meng, C.; Wang, X.; Lü, Z.; Zhang, D.; Chen, W.; Zhao, J.; Yuan, J.; Zhao, Z. Joint Measurements of Terahertz Wave Generation and High-Harmonic Generation from Aligned Nitrogen Molecules Reveal Angle-Resolved Molecular Structures. *Phys. Rev. Lett.* **2015**, *115*, 123002. [[CrossRef](#)] [[PubMed](#)]
22. Dudovich, N.; Smirnova, O.; Levesque, J.; Mairesse, Y.; Ivanov, M.Y.; Villeneuve, D.M.; Corkum, P.B. Measuring and controlling the birth of attosecond XUV pulses. *Nat. Phys.* **2006**, *2*, 781–786. [[CrossRef](#)]
23. Daranciang, D.; Goodfellow, J.; Fuchs, M.; Wen, H.; Ghimire, S.; Reis, D.A.; Loos, H.; Fisher, A.S.; Lindenberg, A.M. Single-cycle terahertz pulses with >0.2 V/Å field amplitudes via coherent transition radiation. *Appl. Phys. Lett.* **2011**, *99*, 141117. [[CrossRef](#)]
24. Schütte, B.; Plünjes, E.; Budzyn, F.; Rossbach, J.; Wieland, M.; Krikunova, M.; Drescher, M.; Gensch, M.; Grimm, O.; Kalms, R. Single-shot terahertz-field-driven X-ray streak camera. *Nat. Photonics* **2009**, *3*, 523.
25. Zhang, X.C.; Shkurinov, A.; Zhang, Y. Extreme terahertz science. *Nat. Photonics* **2017**, *11*, 16–18. [[CrossRef](#)]
26. Popruzhenko, S.V. Coulomb phase in high harmonic generation. *J. Phys. B Atom. Mol. Opt. Phys.* **2018**, *51*, 144006. [[CrossRef](#)]
27. Keldsh, L. Ionization in the field of a strong electromagnetic wave. *Sov. Phys. JETP* **1965**, *20*, 1307–1314.
28. Faisal, F.H.M. Multiple absorption of laser photons by atoms. *J. Phys. B Atom. Mol. Opt. Phys.* **1973**, *6*, L89. [[CrossRef](#)]
29. Reiss, H.R. Effect of an intense electromagnetic field on a weakly bound system. *Phys. Rev. A* **1980**, *22*, 1786–1813. [[CrossRef](#)]
30. Krause, J.L.; Schafer, K.J.; Kulander, K.C. High-order harmonic generation from atoms and ions in the high intensity regime. *Phys. Rev. Lett.* **1992**, *68*, 3535. [[CrossRef](#)] [[PubMed](#)]
31. Winterfeldt, C.; Spielmann, C.; Gerber, G. Colloquium: Optimal control of high-harmonic generation. *Rev. Mod. Phys.* **2008**, *80*, 117–140. [[CrossRef](#)]
32. Lewenstein, M.; Balcou, P.; Ivanov, M.Y.; L’Huillier, A.; Corkum, P.B. Theory of high-harmonic generation by low frequency laser fields. *Phys. Rev. A* **1994**, *49*, 2117–2132. [[CrossRef](#)] [[PubMed](#)]
33. Pfeifer, T.; Gallmann, L.; Abel, M.J.; Neumark, D.M.; Leone, S.R. Single attosecond pulse generation in the multicycle-driver regime by adding a weak second-harmonic field. *Opt. Lett.* **2006**, *31*, 975–977. [[CrossRef](#)] [[PubMed](#)]
34. Takahashi, E.J.; Lan, P.; Mücke, O.D.; Nabekawa, Y.; Midorikawa, K. Infrared Two-Color Multicycle Laser Field Synthesis for Generating an Intense Attosecond Pulse. *Phys. Rev. Lett.* **2010**, *104*, 233901. [[CrossRef](#)] [[PubMed](#)]
35. Hamster, H.; Sullivan, A.; Gordon, S.; White, W.; Falcone, R.W. Subpicosecond, electromagnetic pulses from intense laser-plasma interaction. *Phys. Rev. Lett.* **1993**, *71*, 2725–2728. [[CrossRef](#)] [[PubMed](#)]
36. Xie, X.; Dai, J.; Zhang, X.C. Coherent Control of THz Wave Generation in Ambient Air. *Phys. Rev. Lett.* **2006**, *96*, 075005. [[CrossRef](#)] [[PubMed](#)]
37. Kreß, M.; Löffler, T.; Eden, S.; Thomson, M.; Roskos, H. Terahertz-pulse generation by photoionization of air with laser pulses composed of both fundamental and second-harmonic waves. *Opt. Lett.* **2004**, *29*, 1120–1122. [[CrossRef](#)] [[PubMed](#)]
38. Kim, K.Y.; Taylor, A.J.; Glowina, J.H.; Rodriguez, G. Coherent control of terahertz supercontinuum generation in ultrafast laser-gas interactions. *Nat. Photonics* **2008**, *2*, 605–609. [[CrossRef](#)]
39. Karpowicz, N.; Zhang, X.C. Coherent terahertz echo of tunnel ionization in gases. *Phys. Rev. Lett.* **2009**, *102*, 093001. [[CrossRef](#)] [[PubMed](#)]

40. Zhou, Z.; Zhang, D.; Zhao, Z.; Yuan, J. Terahertz emission of atoms driven by ultrashort laser pulses. *Phys. Rev. A* **2009**, *79*, 063413. [[CrossRef](#)]
41. Faisal, F.H.M. Strong-field physics: Ionization surprise. *Nat. Phys.* **2009**, *5*, 319–320. [[CrossRef](#)]
42. Dura, J.; Camus, N.; Thai, A.; Britz, A.; Hemmer, M.; Baudisch, M.; Senftleben, A.; Schröter, C.D.; Ullrich, J.; Moshhammer, R. Ionization with low-frequency fields in the tunneling regime. *Sci. Rep.* **2013**, *3*, 2675. [[CrossRef](#)] [[PubMed](#)]
43. Yan, T.M.; Popruzhenko, S.V.; Vrakking, M.J.J.; Bauer, D. Low-Energy Structures in Strong Field Ionization Revealed by Quantum Orbits. *Phys. Rev. Lett.* **2010**, *105*, 253002. [[CrossRef](#)] [[PubMed](#)]
44. Becker, W.; Goreslavski, S.P.; Milosevic, D.B.; Paulus, G.G. Low-energy electron rescattering in laser-induced ionization. *J. Phys. B Atom. Mol. Opt. Phys.* **2014**, *47*, 204022. [[CrossRef](#)]
45. Xia, Q.Z.; Ye, D.F.; Fu, L.B.; Han, X.Y.; Liu, J.; Xia, Q.Z.; Ye, D.F.; Fu, L.B.; Han, X.Y.; Liu, J. Momentum Distribution of Near-Zero-Energy Photoelectrons in the Strong-Field Tunneling Ionization in the Long Wavelength Limit. *Sci. Rep.* **2015**, *5*, 11473. [[CrossRef](#)] [[PubMed](#)]
46. Haessler, S.; Caillat, J.; Boutu, W.; Giovanetti-Teixeira, C.; Ruchon, T.; Auguste, T.; Diveki, Z.; Breger, P.; Maquet, A.; Carre, B.; et al. Attosecond imaging of molecular electronic wavepackets. *Nat. Phys.* **2010**, *6*, 200–206. [[CrossRef](#)]
47. Dahlström, J.M.; Fordell, T.; Mansten, E.; Ruchon, T.; Swoboda, M.; Klünder, K.; Gisselbrecht, M.; L’Huillier, A.; Mauritsson, J. Atomic and macroscopic measurements of attosecond pulse trains. *Phys. Rev. A* **2009**, *80*, 033836. [[CrossRef](#)]
48. Diveki, Z.; Guichard, R.; Caillat, J.; Camper, A.; Haessler, S.; Auguste, T.; Ruchon, T.; Carré, B.; Maquet, A.; Taïeb, R.; et al. Molecular orbital tomography from multi-channel harmonic emission in N₂. *Chem. Phys.* **2013**, *414*, 121–129. [[CrossRef](#)]
49. Boutu, W.; Haessler, S.; Merdji, H.; Breger, P.; Waters, G.; Stankiewicz, M.; Frasinski, L.J.; Taieb, R.; Caillat, J.; Maquet, A.; et al. Coherent control of attosecond emission from aligned molecules. *Nat. Phys.* **2008**, *4*, 545–549. [[CrossRef](#)]
50. Kazamias, S.; Balcou, P. Intrinsic chirp of attosecond pulses: Single-atom model versus experiment. *Phys. Rev. A* **2004**, *69*, 063416. [[CrossRef](#)]
51. He, X.; Dahlström, J.M.; Rakowski, R.; Heyl, C.M.; Persson, A.; Mauritsson, J.; L’Huillier, A. Interference effects in two-color high-order harmonic generation. *Phys. Rev. A* **2010**, *82*, 033410. [[CrossRef](#)]
52. Watanabe, S.; Kondo, K.; Nabekawa, Y.; Sagisaka, A.; Kobayashi, Y. Two-color phase control in tunneling ionization and harmonic generation by a strong laser field and its third harmonic. *Phys. Rev. Lett.* **1994**, *73*, 2692–2695. [[CrossRef](#)] [[PubMed](#)]
53. Gütde, J.; Rohleder, M.; Meier, T.; Koch, S.W.; Höfer, U. Time-resolved investigation of coherently controlled electric currents at a metal surface. *Science* **2007**, *318*, 1287–1291. [[CrossRef](#)] [[PubMed](#)]
54. Tulskey, V.A.; Almajid, M.A.; Bauer, D. Two-color phase-of-the-phase spectroscopy with circularly polarized laser pulses. *Phys. Rev. A* **2018**, *98*, 053433. [[CrossRef](#)]
55. Mizoguchi, K.; Furuichi, T.; Kojima, O.; Nakayama, M.; Sakai, K. Intense terahertz radiation from longitudinal optical phonons in GaAs/AlAs multiple quantum wells. *Appl. Phys. Lett.* **2005**, *87*, 093102. [[CrossRef](#)]
56. Shen, Y.C.; Upadhyaya, P.C.; Linfield, E.H.; Beere, H.E.; Davies, A.G. Terahertz generation from coherent optical phonons in a biased GaAs photoconductive emitter. *Phys. Rev. B* **2004**, *69*, 235325. [[CrossRef](#)]
57. Ulbricht, R.; Hendry, E.; Shan, J.; Heinz, T.F.; Bonn, M. Carrier dynamics in semiconductors studied with time-resolved terahertz spectroscopy. *Rev. Mod. Phys.* **2011**, *83*, 543–586. [[CrossRef](#)]
58. Kampfath, T.; Tanaka, K.; Nelson, K.A. Resonant and nonresonant control over matter and light by intense terahertz transients. *Nat. Photonics* **2013**, *7*, 680–690. [[CrossRef](#)]
59. Gragossian, A.; Seletskiy, D.V.; Sheik-Bahae, M. Classical trajectories in polar-asymmetric laser fields: Synchronous THz and XUV emission. *Sci. Rep.* **2016**, *6*, 34973. [[CrossRef](#)] [[PubMed](#)]
60. Salieres, P.; L’Huillier, A.; Lewenstein, M. Coherence control of high-order harmonics. *Phys. Rev. Lett.* **1995**, *74*, 3776–3779. [[CrossRef](#)] [[PubMed](#)]
61. Zaïr, A.; Holler, M.; Guandalini, A.; Schapper, F.; Biegert, J.; Gallmann, L.; Keller, U.; Wyatt, A.S.; Monmayrant, A.; Walmsley, I.A. Quantum path interferences in high-order harmonic generation. *Phys. Rev. Lett.* **2008**, *100*, 143902. [[CrossRef](#)] [[PubMed](#)]
62. Heyl, C.M.; Gütde, J.; Höfer, U.; L’Huillier, A. Spectrally Resolved Maker Fringes in High-Order Harmonic Generation. *Phys. Rev. Lett.* **2011**, *107*, 033903. [[CrossRef](#)] [[PubMed](#)]

63. He, L.; Lan, P.; Zhang, Q.; Zhai, C.; Wang, F.; Shi, W.; Lu, P. Spectrally resolved spatiotemporal features of quantum paths in high-order harmonic generation. *Phys. Rev. A* **2015**, *92*, 043403. [[CrossRef](#)]
64. Carlstrom, S.; Prelikova, J.; Lorek, E.; Larsen, E.W.; Heyl, C.; Palecek, D.; Zigmantas, D.; Schafer, K.J.; Gaarde, M.B.; Mauritsson, J. Spatially and spectrally resolved quantum path interference with chirped driving pulses. *New J. Phys.* **2016**, *18*, 123032. [[CrossRef](#)]
65. Lan, P.; Ruhmann, M.; He, L.; Zhai, C.; Wang, F.; Zhu, X.; Zhang, Q.; Zhou, Y.; Li, M.; Lein, M.; et al. Attosecond Probing of Nuclear Dynamics with Trajectory-Resolved High-Harmonic Spectroscopy. *Phys. Rev. Lett.* **2017**, *119*, 033201. [[CrossRef](#)] [[PubMed](#)]
66. Haessler, S.; Caillat, J.; Salières, P. Self-probing of molecules with high harmonic generation. *J. Phys. B Atom. Mol. Opt. Phys.* **2011**, *44*, 203001. [[CrossRef](#)]
67. Meng, C.; Lu, Z.; Huang, Y.; Wang, X.; Chen, W.; Zhang, D.; Zhao, Z.; Yuan, J. In situ spatial mapping of Gouy phase slip with terahertz generation in two-color field. *Opt. Express* **2016**, *24*, 12301–12309. [[CrossRef](#)] [[PubMed](#)]
68. Feng, S.; Winful, H.G. Physical origin of the Gouy phase shift. *Opt. Lett.* **2001**, *26*, 485–487. [[CrossRef](#)] [[PubMed](#)]
69. Rosca-Pruna, F.; Vrakking, M.J.J. Experimental Observation of Revival Structures in Picosecond Laser-Induced Alignment of I₂. *Phys. Rev. Lett.* **2001**, *87*, 153902. [[CrossRef](#)] [[PubMed](#)]
70. Itatani, J.; Levesque, J.; Zeidler, D.; Niikura, H.; Pepin, H.; Kieffer, J.C.; Corkum, P.B.; Villeneuve, D.M. Tomographic imaging of molecular orbitals. *Nature* **2004**, *432*, 867–871. [[CrossRef](#)] [[PubMed](#)]
71. Kanai, T.; Minemoto, S.; Sakai, H. Quantum interference during high-order harmonic generation from aligned molecules. *Nature* **2005**, *435*, 470–474. [[CrossRef](#)] [[PubMed](#)]
72. Smirnova, O.; Mairesse, Y.; Patchkovskii, S.; Dudovich, N.; Villeneuve, D.; Corkum, P.; Ivanov, M.Y. High harmonic interferometry of multi-electron dynamics in molecules. *Nature* **2009**, *460*, 972–977. [[CrossRef](#)] [[PubMed](#)]
73. McFarland, B.K.; Farrell, J.P.; Bucksbaum, P.H.; Gühr, M. High Harmonic Generation from Multiple Orbitals in N₂. *Science* **2008**, *322*, 1232–1235. [[CrossRef](#)] [[PubMed](#)]
74. Vozzi, C.; Negro, M.; Calegari, F.; Sansone, G.; Nisoli, M.; De Silvestri, S.; Stagira, S. Generalized molecular orbital tomography. *Nat. Phys.* **2011**, *7*, 822–826. [[CrossRef](#)]
75. Yun, H.; Lee, K.M.; Sung, J.H.; Kim, K.T.; Kim, H.T.; Nam, C.H. Resolving Multiple Molecular Orbitals Using Two-Dimensional High-Harmonic Spectroscopy. *Phys. Rev. Lett.* **2015**, *114*, 153901. [[CrossRef](#)] [[PubMed](#)]
76. Le, A.T.; Lucchese, R.R.; Tonzani, S.; Morishita, T.; Lin, C.D. Quantitative rescattering theory for high-order harmonic generation from molecules. *Phys. Rev. A* **2009**, *80*, 013401. [[CrossRef](#)]
77. Kjeldsen, T.K.; Madsen, L.B. Strong-field ionization of diatomic molecules and companion atoms: Strong-field approximation and tunneling theory including nuclear motion. *Phys. Rev. A* **2005**, *71*, 23411. [[CrossRef](#)]
78. Tong, X.M.; Zhao, Z.X.; Lin, C.D. Theory of molecular tunneling ionization. *Phys. Rev. A* **2002**, *66*, 033402. [[CrossRef](#)]
79. Pavičić, D.; Lee, K.F.; Rayner, D.M.; Corkum, P.B.; Villeneuve, D.M. Direct Measurement of the Angular Dependence of Ionization for N₂, O₂ and CO₂ in Intense Laser Fields. *Phys. Rev. Lett.* **2007**, *98*, 243001. [[CrossRef](#)] [[PubMed](#)]
80. Thomann, I.; Lock, R.; Sharma, V.; Gagnon, E.; Pratt, S.T.; Kapteyn, H.C.; Murnane, M.M.; Li, W. Direct measurement of the angular dependence of the single-photon ionization of aligned N₂ and CO₂. *J. Phys. Chem. A* **2008**, *112*, 9382–9386. [[CrossRef](#)] [[PubMed](#)]
81. You, Y.; Oh, T.; Fallahkhair, A.; Kim, K. Alignment-dependent terahertz radiation in two-color photoionization of molecules. *Phys. Rev. A* **2013**, *87*, 035401. [[CrossRef](#)]
82. Huang, Y.; Meng, C.; Zhao, J.; Wang, X.; Lü, Z.; Zhang, D.; Yuan, J.; Zhao, Z. High-harmonic and terahertz wave spectroscopy (HATS) for aligned molecules. *J. Phys. B Atom. Mol. Opt. Phys.* **2016**, *49*, 235601. [[CrossRef](#)]
83. Itatani, J.; Zeidler, D.; Levesque, J.; Spanner, M.; Villeneuve, D.M.; Corkum, P.B. Controlling High Harmonic Generation with Molecular Wave Packets. *Phys. Rev. Lett.* **2005**, *94*, 123902. [[CrossRef](#)] [[PubMed](#)]
84. Abdurrouf, A.; Faisal, F. Theory of intense-field dynamic alignment and high-order harmonic generation from coherently rotating molecules and interpretation of intense-field ultrafast pump-probe experiments. *Phys. Rev. A* **2009**, *79*, 023405. [[CrossRef](#)]

85. Lein, M.; Hay, N.; Velotta, R.; Marangos, J.P.; Knight, P.L. Role of the Intramolecular Phase in High-Harmonic Generation. *Phys. Rev. Lett.* **2002**, *88*, 183903. [[CrossRef](#)] [[PubMed](#)]
86. Yoshii, K.; Miyaji, G.; Miyazaki, K. Retrieving Angular Distributions of High-Order Harmonic Generation from a Single Molecule. *Phys. Rev. Lett.* **2011**, *106*, 013904. [[CrossRef](#)] [[PubMed](#)]
87. Bertrand, J.B.; Wörner, H.J.; Hockett, P.; Villeneuve, D.M.; Corkum, P.B. Revealing the Cooper minimum of N₂ by Molecular Frame High-Harmonic Spectroscopy. *Phys. Rev. Lett.* **2012**, *109*, 143001. [[CrossRef](#)] [[PubMed](#)]
88. Jin, C.; Bertrand, J.B.; Lucchese, R.R.; Wörner, H.J.; Corkum, P.B.; Villeneuve, D.M.; Le, A.T.; Lin, C.D. Intensity dependence of multiple orbital contributions and shape resonance in high-order harmonic generation of aligned N₂ molecules. *Phys. Rev. A* **2012**, *85*, 013405. [[CrossRef](#)]
89. Kim, K.Y. Generation of coherent terahertz radiation in ultrafast laser-gas interactions. *Phys. Plasmas* **2009**, *16*, 056706. [[CrossRef](#)]
90. Zimmermann, B.; Lein, M.; Rost, J.M. Analysis of recombination in high-order harmonic generation in molecules. *Phys. Rev. A* **2005**, *71*, 033401. [[CrossRef](#)]
91. Spanner, M.; Bertrand, J.B.; Villeneuve, D.M. In situ attosecond pulse characterization techniques to measure the electromagnetic phase. *Phys. Rev. A* **2016**, *94*, 023825. [[CrossRef](#)]
92. Bellini, M.; Lynga, C.; Tozzi, A.; Gaarde, M.B.; Hansch, T.W.; Huillier, A.L.; Wahlstrom, C.G. Temporal Coherence of Ultrashort High-Order Harmonic Pulses. *Phys. Rev. Lett.* **1998**, *81*, 337. [[CrossRef](#)]
93. Huismans, Y.; Rouzee, A.; Gijsbertsen, A.; Jungmann, J.H.; Smolkowska, A.S.; Logman, P.S.W.M.; Lepine, F.; Cauchy, C.; Zamith, S.; Marchenko, T.; et al. Time-Resolved Holography with Photoelectrons. *Science* **2011**, *331*, 61–64. [[CrossRef](#)] [[PubMed](#)]
94. Meckel, M.; Staudte, A.; Patchkovskii, S.; Villeneuve, D.M.; Corkum, P.B.; Dorner, R.; Spanner, M. Signatures of the continuum electron phase in molecular strong-field photoelectron holography. *Nat. Phys.* **2014**, *10*, 594–600. [[CrossRef](#)]
95. Huang, Y.; Meng, C.; Zhao, J.; Wang, X.; Lv, Z.; Guo, Q.; Zhang, D.; Yuan, J.; Zhao, Z. Phase dependent high-harmonics and terahertz-wave spectroscopy (HATS) from aligned carbon dioxide. In Proceedings of the 2016 41st International Conference on Infrared, Millimeter, and Terahertz Waves (IRMMW-THz), Copenhagen, Denmark, 25–30 September 2016; pp. 1–2.
96. Huang, Y.; Zhao, J.; Shu, Z.; Liu, L.; Dong, W.; Wang, X.; Lü, Z.; Zhang, D.; Chang, C.; Yuan, J.; et al. Molecular channel-controlled attosecond burst with THz benchmark. in submission.
97. Brabec, T.; Krausz, F. Intense few-cycle laser fields: Frontiers of nonlinear optics. *Rev. Mod. Phys.* **2000**, *72*, 545–591. [[CrossRef](#)]
98. Hu, H.; Li, N.; Liu, P.; Li, R.; Xu, Z. Pure Even Harmonic Generation from Oriented CO in Linearly Polarized Laser Fields. *Phys. Rev. Lett.* **2017**, *119*, 173201. [[CrossRef](#)] [[PubMed](#)]
99. Frumker, E.; Kajumba, N.; Bertrand, J.B.; Wörner, H.J.; Hebeisen, C.T.; Hockett, P.; Spanner, M.; Patchkovskii, S.; Paulus, G.G.; Villeneuve, D.M.; et al. Probing Polar Molecules with High Harmonic Spectroscopy. *Phys. Rev. Lett.* **2012**, *109*, 233904. [[CrossRef](#)] [[PubMed](#)]
100. Alexandrov, L.N.; Emelin, M.Y.; Ryabikin, M.Y. Unidirectional current excitation in tunneling ionization of asymmetric molecules. *Phys. Rev. A* **2013**, *87*, 013414. [[CrossRef](#)]
101. Liu, L.; Zhao, J.; Yuan, J.; Zhao, Z. Local-microfield enhancement of high-order harmonic generation and the associated electron dynamics. *Sci. Sin. Phys. Mech. Astron.* **2017**, *47*, 033006. [[CrossRef](#)]
102. Dong, W.; Huang, Y.; Liu, J.; Liu, L.; Zhao, J.; Zhao, Z. Laser-induced ionic excitation in one-dimensional model H₂. *J. Phys. B Atom. Mol. Opt. Phys.* **2017**, *50*, 234001. [[CrossRef](#)]
103. Ghimire, S.; Dichiara, A.D.; Sistrunk, E.; Agostini, P.; Dimauro, L.F.; Reis, D.A. Observation of high-order harmonic generation in a bulk crystal. *Nat. Phys.* **2010**, *7*, 138–141. [[CrossRef](#)]
104. Vampa, G.; McDonald, C.R.; Orlando, G.; Klug, D.D.; Corkum, P.B.; Brabec, T. Theoretical Analysis of High-Harmonic Generation in Solids. *Phys. Rev. Lett.* **2014**, *113*, 073901. [[CrossRef](#)] [[PubMed](#)]
105. Schubert, O.; Hohenleutner, M.; Langer, F.; Urbanek, B.; Lange, C.; Huttner, U.; Golde, D.; Meier, T.; Kira, M.; Koch, S.W.; et al. Sub-cycle control of terahertz high-harmonic generation by dynamical Bloch oscillations. *Nat. Photonics* **2014**, *8*, 119–123. [[CrossRef](#)]
106. Vampa, G.; Hammond, T.J.; Thire, N.; Schmidt, B.E.; Legare, F.; McDonald, C.R.; Brabec, T.; Corkum, P.B. Linking high harmonics from gases and solids. *Nature* **2015**, *522*, 462–464. [[CrossRef](#)] [[PubMed](#)]

107. Luu, T.T.; Garg, M.; Kruchinin, S.Y.; Moulet, A.; Hassan, M.T.; Goulielmakis, E. Extreme ultraviolet high-harmonic spectroscopy of solids. *Nature* **2015**, *521*, 498. [[CrossRef](#)] [[PubMed](#)]
108. Hohenleutner, M.; Langer, F.; Schubert, O.; Knorr, M.; Huttner, U.; Koch, S.W.; Kira, M.; Huber, R. Real-time observation of interfering crystal electrons in high-harmonic generation. *Nature* **2016**, *523*, 572. [[CrossRef](#)] [[PubMed](#)]
109. Ndabashimiye, G.; Ghimire, S.; Wu, M.; Browne, D.A.; Schafer, K.J.; Gaarde, M.B.; Reis, D.A. Solid-state harmonics beyond the atomic limit. *Nature* **2016**, *534*, 520. [[CrossRef](#)] [[PubMed](#)]
110. Jin, Q.; E, Y.; Williams, K.; Dai, J.; Zhang, X.C. Observation of broadband terahertz wave generation from liquid water. *Appl. Phys. Lett.* **2017**, *111*, 071103. [[CrossRef](#)]
111. Evarestov, R.A. *Quantum Chemistry of Solids: The LCAO First Principles Treatment of Crystals*; Springer: Berlin/Heidelberg, Germany, 2007.
112. Wu, M.; Ghimire, S.; Reis, D.A.; Schafer, K.J.; Gaarde, M.B. High-harmonic generation from Bloch electrons in solids. *Phys. Rev. A* **2015**, *91*, 043839. [[CrossRef](#)]
113. Liu, L.; Zhao, J.; Dong, W.; Liu, J.; Huang, Y.; Zhao, Z. Spatial coherence in high-order-harmonic generation from periodic solid structures. *Phys. Rev. A* **2017**, *96*, 053403. [[CrossRef](#)]
114. Osika, E.N.; Chacón, A.; Ortmann, L.; Suárez, N.; Pérez-Hernández, J.A.; Szafran, B.; Ciappina, M.F.; Sols, F.; Landsman, A.S.; Lewenstein, M. Wannier-Bloch Approach to Localization in High-Harmonics Generation in Solids. *Phys. Rev. X* **2017**, *7*, 021017. [[CrossRef](#)]
115. Tancogne-Dejean, N.; Mücke, O.D.; Kärtner, F.X.; Rubio, A. Impact of the Electronic Band Structure in High-Harmonic Generation Spectra of Solids. *Phys. Rev. Lett.* **2017**, *118*, 087403. [[CrossRef](#)] [[PubMed](#)]
116. Tancogne-Dejean, N.; Rubio, A. Atomic-like high-harmonic generation from two-dimensional materials. *Sci. Adv.* **2018**, *4*, eaao5207. [[CrossRef](#)] [[PubMed](#)]
117. Thrane, L.; Jacobsen, R.H.; Jepsen, P.U.; Keiding, S.R. THz reflection spectroscopy of liquid water. *Chem. Phys. Lett.* **1995**, *240*, 330–333. [[CrossRef](#)]
118. Tielrooij, K.; Garcia-Araez, N.; Bonn, M.; Bakker, H. Cooperativity in Ion Hydration. *Science* **2010**, *328*, 1006–1009. [[CrossRef](#)] [[PubMed](#)]
119. Tanaka, K.; Harada, K.; Yamada, K.M. THz and Submillimeter-wave Spectroscopy of Molecular Complexes. In *Handbook of High-Resolution Spectroscopy*; John Wiley & Sons, Ltd.: Chichester, UK, 2011.



© 2019 by the authors. Licensee MDPI, Basel, Switzerland. This article is an open access article distributed under the terms and conditions of the Creative Commons Attribution (CC BY) license (<http://creativecommons.org/licenses/by/4.0/>).